Int. J. Electrochem. Sci., 17 **(2022)** Article Number: 22112, doi: 10.20964/2022.11.17

International Journal of
ELECTROCHEMICAL
SCIENCE
www.electrochemsci.org

Electrocatalytic Heterogeneous Oxidation of Alcohols (Methanol, Ethanol and Isopropanol) Using GC-Modified Electrodes with Unsymmetrical Ni^{II}-Schiff Base Complex

Wassila Derafa[1,2], *Djouhra Aggoun*[2,3,*], *Ali Ourari*[2]

[1] Chemistry Department, College of Science, Jouf University, Sakaka 72388, Saudi Arabia.
[2] Laboratory of Electrochemistry, Molecular Engineering and Redox Catalysis, Department of Process Engineering, Faculty of technology, University of Ferhat Abbas, Setif-1, 19000, Algeria.
[3] Chemistry Department, Faculty of sciences, University Ferhat Abbas, Setif-1, 19000 Algeria.
[*]E-mail: aggoun81@yahoo.fr

Received: 9 April 2022 / *Accepted:* 7 June 2022 / *Published:* 10 October 2022

In this work, the studied Nickel Schiff-base complex was synthesized in methanol medium using dehydroacetic acid (DHA), ethylene diamine in presence of an excess of pyridine and tetrahydrate salt of nickel chloride. The properties of this new complex were determined via infrared (IR), electronic spectrum (UV-Vis.), elemental analysis (CHN), X-ray photoelectron spectroscopy (XPS) and cyclic voltammetry (CV). The synthesized nickel monomer was electrodeposited on glassy carbon (GC), Indium tin oxide (ITO) and fluorine tin oxide (FTO) as conductive electrodes by anodic oxidation in alkaline solutions yielding electroactive films strongly adhered. These materials, currently called modified electrodes (noted ME), were obtained by the successive cycling at the appropriate potentials showing a typical voltammetric response such as Ni(III)/Ni(II) redox couple. Accordingly, the poly-[Ni(II)-L-pyridine]Cl modified electrodes were characterized by cyclic voltammetry whereas the surface morphology of these films was characterized by scanning electron microscopy (SEM) and X-ray photoelectron spectroscopy (XPS). The films prepared onto glassy carbon electrode display a powerful and persistent indirect catalytic activity towards the electro-oxidation of some aliphatic alcohols of short chain. The electro-oxidation reaction of methanol (MeOH), ethanol (EtOH) and iso-propanol (^{i}PrOH) has been investigated by cyclic voltammetry and change with the number of voltammetric scans and concentrations of the used alcohol. A virtuous electrocatalytic activity was obviously observed showing that the oxidation reaction was illustrated by a peak current which increases progressively as the alcohol concentration increases.

Keywords: Unsymmetrical Ni-Schiff base complex, Modified electrodes, Aliphatic alcohols, Heterogeneous electro-oxidation.

1. INTRODUCTION

One of the most significant reactions in organic chemistry and the most transformations in chemical industries is the oxidation of alcohols leading to the formation of their corresponding carbonyl compounds [1]. This reaction can produce aldehydes and carboxylic acids by using primary alcohols, or they can be oxidized to yield ketones in the case of secondary alcohols [2]. During the last recent decades, the catalytic oxidation methods that using ambient air, oxygen or hydrogen peroxide as an oxidant have been widely investigated in the literature [3]. Several essential factors that used to control these oxidation reaction rates are the subject of numerous earlier studies [4]. However, in the point of view of their pivotal role in redox chemistry, innumerable studies using Schiff base complexes containing electro-polymerizable groups such as porphyrins, cyclam, salen and phthalocyanines were extensively described in the literature [5-9]. Based on these classes of compounds, the resulting modified electrode surfaces with these polymeric films were found to be very interesting heterogeneous electrocatalysts towards the electro-oxidation of alcohols [10-12]. Also, it seems that they offer effective modified materials for the electrocatalytic oxidation of different aliphatic and aromatic alcohols [13,14].

Although the electrocatalytic properties of nickel Schiff bases complexes, and typical behavior of the prepared electropolymerized films in alkaline media have been recently well studied [15-17]. During the last decade, it has been shown that polymeric nickel complexes derived from Salen Schiff base ligand, electrodeposited films in alkaline media to yield stable modified electrodes, were successfully used to catalyze the oxidation reaction of several alcohols [18-20]. On the other hand, few data exist on the electrochemical behavior and electrocatalytic activation of alcohols of unsymmetrical metal Schiff base complexes [21]. The oxidation mechanisms of methanol [22], ethanol [23] and iso-propanol [24] have been widely studied in alkaline media using cyclic voltammetry. Especially, 2-propanol alcohol has great interest toward electrochemical oxidation due to its particular molecular structure as the smallest secondary alcohol and less toxic compared to methanol alcohol [25,26].

The purpose of this paper is to explore the diverse investigations of alcohols electro-oxidation activity using new techniques implicating the modification of the electrode surfaces using new molecular materials of coordination chemistry like thin films of nickel unsymmetrical Schiff base complex. The structure of the prepared nickel complex was elucidated using EA, IR, UV-Vis, CV and XPS techniques. The electro-polymerization of this synthesized monomer is accomplished by cyclic voltammetry using continuous cycling in the range of potentials appropriately chosen. The obtained modified electrodes (ME) were also characterized by CV, XPS and SEM methods. The structural representation of designing the expected nickel complex is shown in the following Scheme 1:

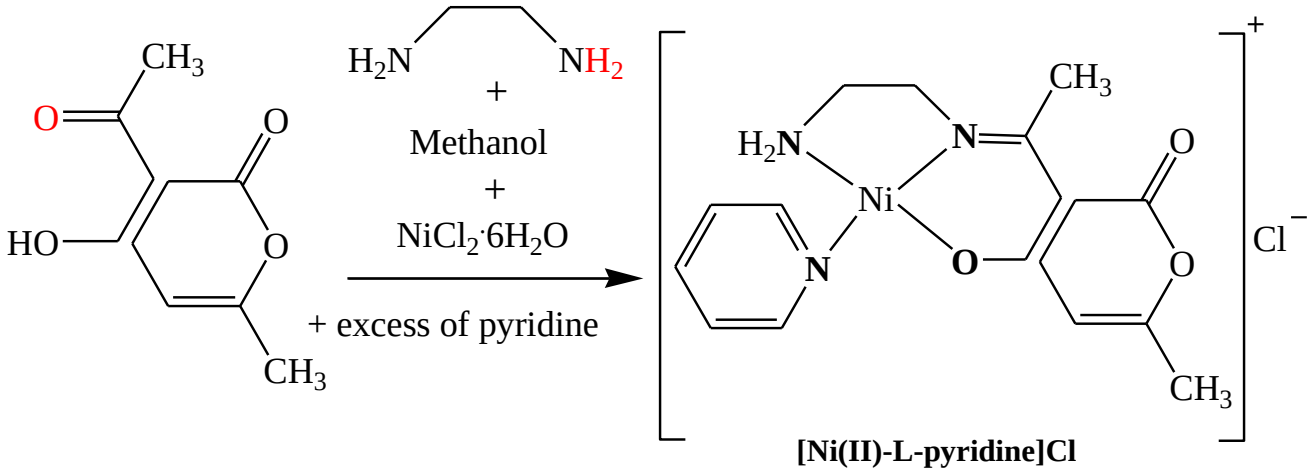

[Ni(II)-L-pyridine]Cl

With L: 3-[1-(2-Amino-ethylimino)-ethyl]-4-hydroxy-6-methyl-pyran-2-one.

Scheme 1. Synthetic route leading to the formation of the nickel complex.

2. EXPERIMENTAL

2.1. Physical measurements

All chemicals used were analytical grade of Aldrich chemical origin and were used without further purification. According to the published procedures, the monomer [Ni(II)-L-pyridine]Cl complex was synthesized by template condensation of dehydroacetic acid, pyridine and ethylenediamine with $NiCl_2 \cdot 6H_2O$ dissolved as well in methanol.

IR spectrum was recorded on Perkin Elmer 1000-FT-IR Spectrometer using KBr disks. The electronic spectrum was recorded on a Unicam UV-300 Spectrophotometer having 1 cm as a path length cell. XPS measurements were obtained using a MULTILAB 2000 (THERMO VG) spectrometer equipped with an Al K-X-ray source (1486.6 eV). The obtained high-resolution spectra were carried out in constant pass energy mode (100 and 20 eV, respectively). The C 1s peak at 284.6 eV was used to precise charging effects.

Cyclic voltammograms were carried out in a conventional three-electrode cell and a VOLTALAB system with PGSTAT 300PZ. For electro-polymerization experiments, the poly-[Ni(II)-L-pyridine]Cl films were grown from a solution of 1 mM of [Ni(II)-L-pyridine]Cl monomer in water, containing 0.1 M sodium chloride (NaCl) using cyclic voltammetry. A saturated calomel electrode (SCE) wire was reference electrode, the working electrode was glassy carbon (GC, area = 0.03 cm^2) and the counter electrode was a platinum wire. The semi-transparent working electrodes used in this study are indium tin oxide (ITO) and fluorine tin oxide (FTO), these electrodes were prepared by cutting the glass in its appropriate size (active area = 1 cm^2).

2.2. Synthesis

According to the published template condensation procedures [27], the studied nickel complex was obtained by mixing stoichiometric quantities of 168 mg of 3-acetyl-2-hydroxy-6-methyl-4*H*-pyran-4-one (DHA) (1 mmol) with 238 mg of hexa-hydrated nickel chloride ($NiCl_2 \cdot 6H_2O$) (1mmole). To this mixture was added 60 mg of ethylenediamine (1mmol) dissolved in methanol solution (10 ml) and at that time 158 mg of pyridine (2 mmol) was as well added. After two hours of reaction, the sky-blue precipitate was recovered by filtration, washed by using cooled methanol and diethyl ether and finally dried over $CaCl_2$ yielding sky-blue powder with 75% as yield. M.p.: >260 °C. UV–Vis. (DMF) $\lambda_{max(n)}$ (nm), $\varepsilon_{max(n)}$ [M^{-1} cm^{-1}]: $\lambda_{max(1)}$ (279), $\varepsilon_{max(1)}$ [3250]; $\lambda_{max(2)}$ (312), $\varepsilon_{max(2)}$ [1000]; $\lambda_{max(3)}$ (378), $\varepsilon_{max(3)}$ [400]. FT-IR (KBr) ν_x (cm^{-1}): νNH_2 (free amine) 3338, 3274 cm^{-1}, νO=C–O 1723, νC=N 1641, νCl_2 1306, νNi–O–C1393, νNi–N 1343, ν(M–O) 420–550, ν(M–N) 600–700. Elemental analysis: Anal. Calc. for $C_{15}H_{18}N_3O_3ClNi \cdot 2.5\ H_2O$: C, 42.14; H, 5.42; N, 8.29. Found: C, 42.09; H, 5.34; N, 8.43 %.

3. RESULTS AND DISCUSSION

3.1. Spectral characterization

The FT-IR spectrum of [Ni(II)-L-pyridine]Cl complex undoubtedly displays two bands at 3338 and 3274 cm^{-1}. The appearance of two absorption bands in this region were ascribed to the free amine group (ν_{NH2}) vibrations. The band observed at 1723 cm^{-1} was ascribed to the vibration ($\nu_{O=C-O}$) characterized the lactone function [28]. A clearly strong and sharp absorption band was found at 1641 cm^{-1} that can be attributed to the azomethine ($\nu_{C=N}$) group of the tridentate Schiff base [29]. The presence of chlorine as counter anion is confirmed by the presence of a band at about 1005 cm^{-1}. Adding to this, the formation of the Ni complex was also reinforced by the appearance of the (ν_{Ni-N}) and (ν_{Ni-O}) absorption bands in the regions 420–550 and 600–700 cm^{-1}, respectively. This information is indicative confirming that the phenolic oxygen and azomethine nitrogen atoms are involved in the coordination process generating the formation of the obtained nickel complex [30]. The UV-Vis. spectrum of [Ni(II)-L-pyridine]Cl complex, recorded in DMF solutions, presents two main absorption bands. The intense one observed in the region between 270 and 350 nm is principally ascribed to intra-ligand n–π* transitions. The broader band in the 380–480 nm range is probably attributed to the ligand to metal charge transfer (LMCT) transitions [31].

3.2. Electrochemistry

3.2.1. Preparation of Modified GC-Electrodes (poly-[Ni(II)-L-pyridine]Cl/GCE)

Modification of GC electrode was carried out by electropolymerization of [Ni(II)-L-pyridine]Cl in solution by multiple scan cyclic voltammetry.

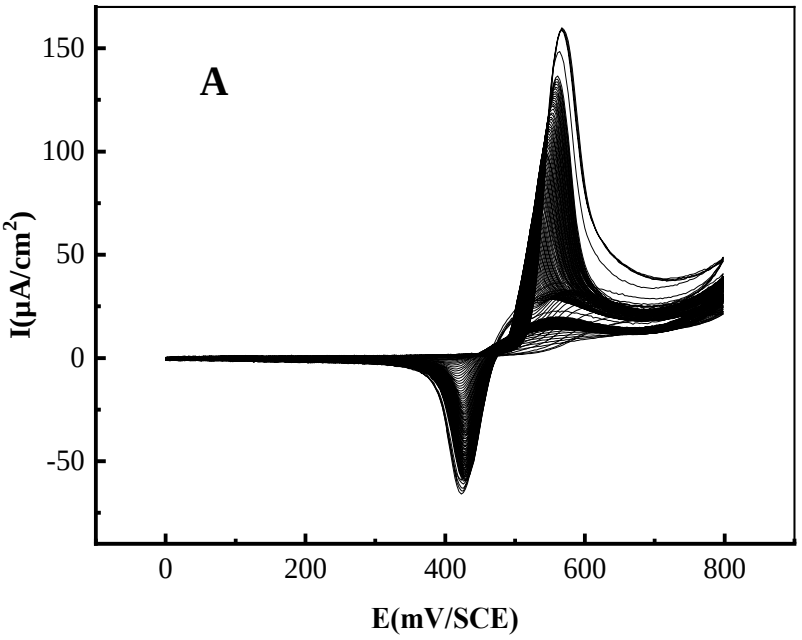
A
150
100
50
0
-50
I(μA/cm2)
0
200
400
600
800
E(mV/SCE)

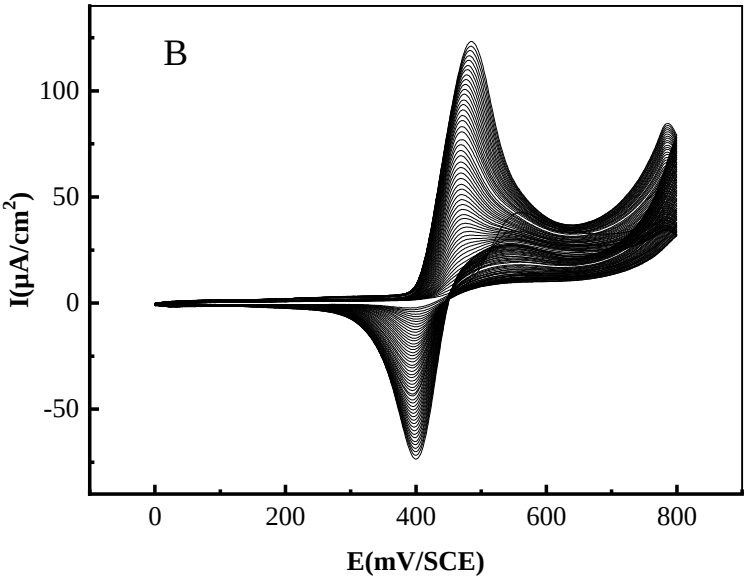
B
100
50
0
-50
I(μA/cm2)
0
200
400
600
800
E(mV/SCE)

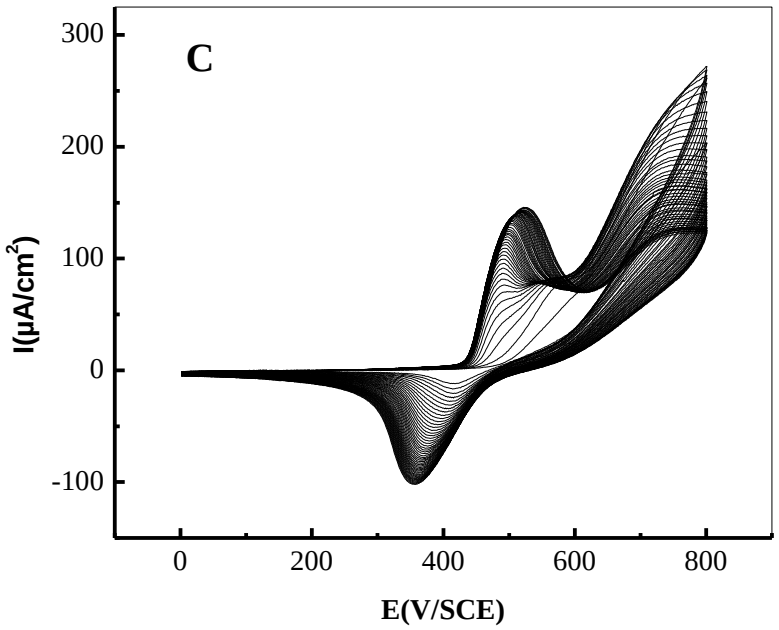

Figure 1. Cyclic voltammograms of 0.1 mM of **[Ni(II)-L-pyridine]Cl** complex at GC electrode in 0.1 M NaOH (pH=11) modified with: **(A)** 100 cycle at 50 mV/s, **(B)** 50 cycle at 50 mV/s, **(C)** 50 cycle at 25 mV/s.

The potential was continuously cycled between 0 and 0.8 V using GC electrode immersed in monomer aqueous solution containing 1 mM [Ni(II)-L-pyridine]Cl and 0.1 M NaOH (pH = 11). Two scan rates were used to prepare these modified electrodes; 50 mV/s (with 100 (curve A) and 50 (curve B) cyclical scan) and 50 cycles were prepared at 25 mV/s. The obtained electroactive films under continuous anodic electro-polymerization cycling were shown in Fig. 1. The Ni^{2+} to Ni^{3+} redox system response was obtained during the first cyclical scan which increases when increasing the potential scans becoming well defined redox couple. Accordingly, in this polymeric film, the detected anodic and cathodic peaks are remaining to the both redox reactions: $Ni^{2+} \rightarrow Ni^{3+} + 1e^-$ (Oxidation reaction at a potential of +0.490 V/SCE) and $Ni^{3+} + 1e^- \rightarrow Ni^{2+}$ (Reduction reaction observed around +0.353 V/SCE), respectively.

The continuous increase in the amplitude of this system confirms the formation of film as a result of the anodic oxidation deposition of the Schiff base nickel complex. The mechanism of electro-oxidative deposition of the nickel complex is until now not clearly established. By the same manner in literature, the electro-polymerization of the copper complex was performed yielding electroactive polymeric films which were found to be very interesting for their useful electrocatalytic properties [32]. At this level, we can also note the electro-oxidative polymerization of a 3-[1-(2-amino-phenylimino)-ethyl]-6-methylpyran-2,4-dione Schiff base ligand studied by U.S. Yousef [33,34].

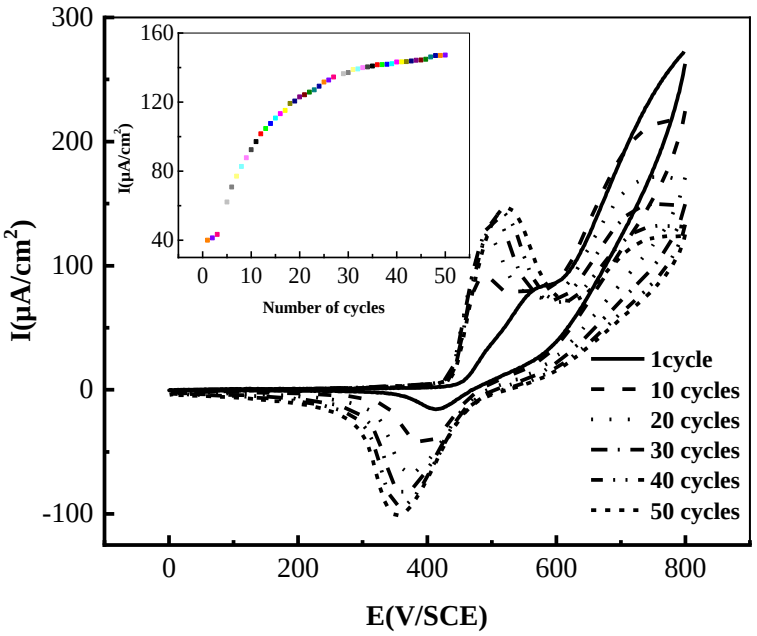

Figure 2. Dependence of anodic peak current of the film of nickel complex on the number of cycles.

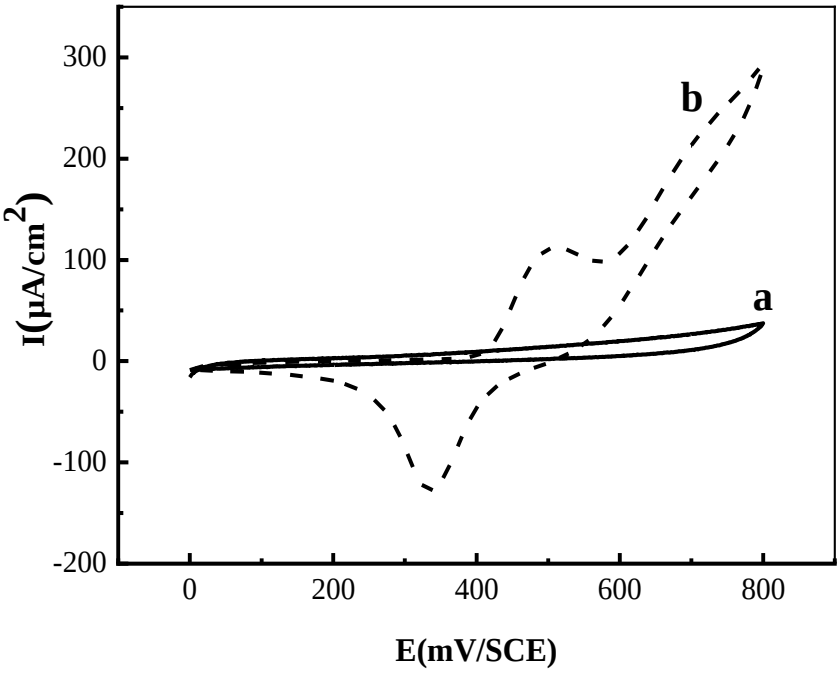

Figure 3. Cyclic voltammograms of (a) unmodified and (b) poly-[Ni(II)-L-pyridine]Cl/GC modified electrode prepared by 50 electro-polymerizing scans in 0.1 M NaOH solution (pH = 11). Scan rate: 25 mV/s.

The intensity of the number of scans does increase linearly over the first 10 electropolymerizing scans (and then increases but not linearly), indicating that the electro-polymerization process progresses

during the cycling of the potential. At the initial stage (1–15 cycles), the nickel film grows very slowly. We think that the retarding reaction process could be imputable to the difficulties in nucleation phenomenon of a new phases formed from nickel compound.

The obtained polymeric film showed high adherence onto the glassy carbon surface. When a poly-[Ni(II)-L-pyridine]Cl/GC electrode is transferred in fresh a 0.1 M NaOH solution, no containing monomer, the cyclic voltammograms resulting showed the typical response of the Ni(II)/Ni(III) redox couple (Fig. 3b) [35,36]. In order to check the electrochemical stability of this polymeric film, its electrochemical response was continuously cycled between 0.0 and +0.8 V using 100 mV/s as scan rate and the cyclic voltammogram obtained was then registered after each 5 cycles.

3.2.2. The Effect of Scan Rate

The effect of the scan rate on poly-[Ni(II)-L-pyridine]Cl/GC modified electrode peak current was investigated. Fig. 4A shows the cyclic voltammograms obtained for a poly-[Ni(II)-L-pyridine]Cl/GC electrode in 0.1 M NaOH solution with various scan rates in the potentials range going from 0.0 to 0.8 V/s. As shown, as the values of scan rate increasing, the anodic peak potential present an important shifting to the more positive potentials. On the other hand, the cathodic peak potential showed as well the same shifting but, in the opposite side converging to the more negative potentials. In all voltammograms, the observed peak-to-peak separation (ΔEp) were found to be more than 100 mV. Furthermore, the present peak currents seem to obey to a linear dependence with the square root of the scan rate (Fig. 4B). These obtained results seem validate with modified electrodes presenting high loadings when the poly-[Ni(II)-L-pyridine]Cl/GC film is electrodeposited. In this case, a relative slow redox transition between the substrate and the nickel redox centers was noted.

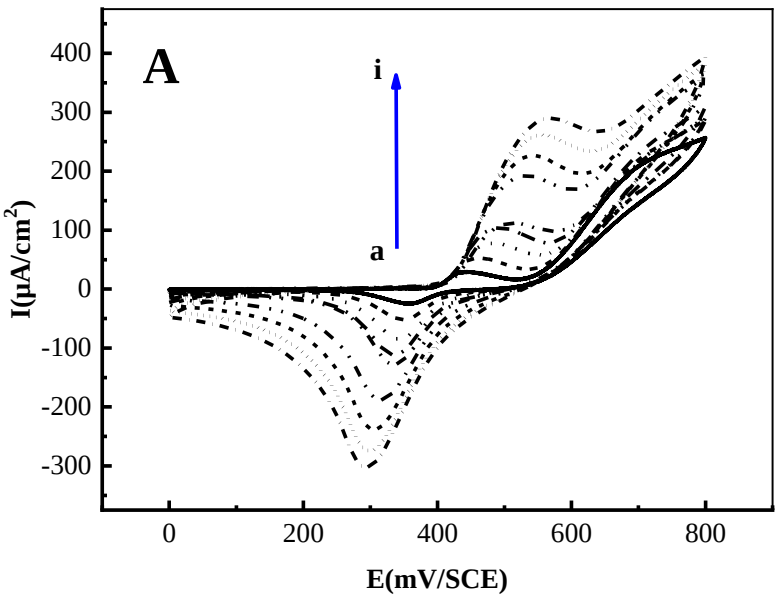

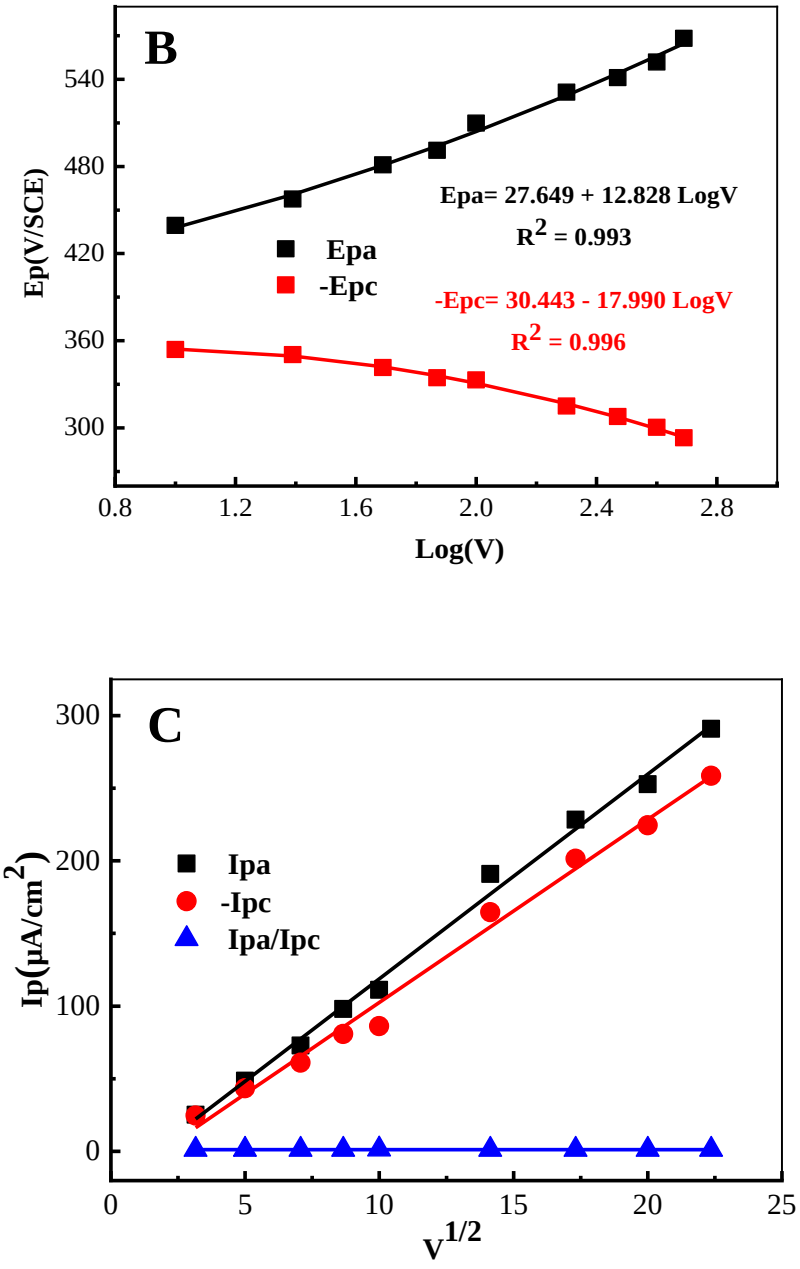

Figure 4. (A) Cyclic voltammetric response of GC electrode modified with a film of [Ni(II)-L-pyridine]Cl in 0.1 M NaOH (pH = 11), at the following scan rates: (a) 10 mV/s; (b) 25 mV/s; (c) 50 mV/s; (d) 75 mV/s; (e) 100 mV/s; (f) 200 mV/s; (j) 300 mV/s; (h) 400 mV/s and (i) 500 mV/s. (B) Laviron's plot showing the dependence of the peak potential on the logarithm of scan rate.(C) plots of anodic and cathodic peak currents versus the square root of potential scan rate.

As can be seen in Fig. 4, a linear relationship of the peak current with $v^{1/2}$ is well observed. This linearity can be explained by charge transfer limited by the diffusion of hydroxyls (OH^-) ions dispersed in the heart of the film. On the other hand, in the scan rate range going from 10 to 200 mV/s, the half anodic peak values are slighter than those expected for a surface of limited system, i.e., 85,9 mV for a

process involving only one electron. This remarqued result suggests the presence of strong attractive interactions between the redox sites inside the polymer film [37,38].

Fig. 4B shows a plot of Ep versus log *v*, the anodic peak shows a potential shifting towards the more positive values, whereas the cathodic peak is additionally shifted towards the more negative potentials. Furthermore, the electron transfer coefficient and the charge transfer rate constant can be evaluated from cyclic voltammetric responses by using the Laviron equations [39].

Fig. 4C shows a plot of Ipc versus $v^{1/2}$. The obtained linearity suggests a diffusion process of poly-[Ni(II)-L-pyridine]Cl/GC probably associated to counter-anion diffusion into and out of the modified electrode [40-42]. Similar voltammograms have also been obtained by modified electrodes characterized by high loadings with poly-[Ni^{II}-DHS] films presenting a relative slow redox transition between the substrate and the nickel redox centers [43].

3.2.3. Preparation of Modified ITO and FTO Electrodes (poly-[Ni(II)-L-pyridine]Cl/ITO or FTO)

Fig. 5 (A) shows the evolution of the cyclic voltammograms from 0.1 M NaOH aqueous solution containing 1 mM of nickel complex in order to electrodeposit its polymer film onto ITO transparent electrode with 100 cyclical scans between 0 to 0.8 V/SCE using 100 mVs^{-1} as scan rate. Consequently, well-defined peaks appearing at 0.4 V that can be ascribed to the Ni^{3+}/ Ni^{2+} redox system [44]. This obtained potential practically is consistent with those obtained in the literature for the electrodeposited Ni(II) complexes onto ITO surface [45]. The formation of a film on the ITO electrode surface is confirmed by the continuous increase of the current peaks. Similar behavior was also observed with FTO transparent electrode under the same experimental conditions (see Fig. 7. (A)).

Nevertheless, the electropolymerizing voltammograms of the [Ni(II)-L-pyridine]Cl show by integration of the oxidation wave for any cycle and the total amount of exchanged charge, noted *Q*ox, was determined. For 50 cyclical scans, a total charge of 1.6 mC/cm^2 was obtained. The plot of the charge exchange versus number of cycles is shown in Fig. 6 (See inset). After 100 cycles, the surface coverage was estimated to be equal to Γ=1.7 x 0^{-8} mol/cm^2. The same shape of the peak is found when the electrode is freshly obtained from the mother solution, followed by an abundant rinsing with water, drying with air flow, and then used as working electrode, without any traces of monomer (Ni complex). This obviously designates that the obtained film covering the surface of the electrode is endowed with a good adherence.

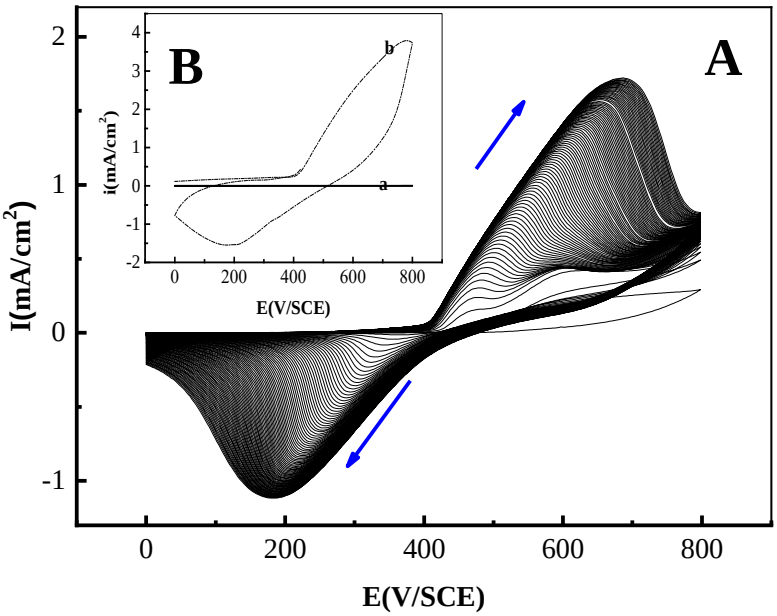

Figure 5. (A) Synthesis of electroactive film of nickel compounds (100 cycles) on ITO in alkaline solution (10^{-1} M NaCl, 10^{-1} M NaOH, pH = 11) containing 10^{-3} M of [Ni(II)-L-pyridine]Cl, v = 100 mVs^{-1}. Inset (B): unmodified ITO electrode (a), cyclic voltammogram of the film of nickel compounds (100 cycles) in the alkaline solution; v = 100 V s^{-1}, modified ITO electrode (b).

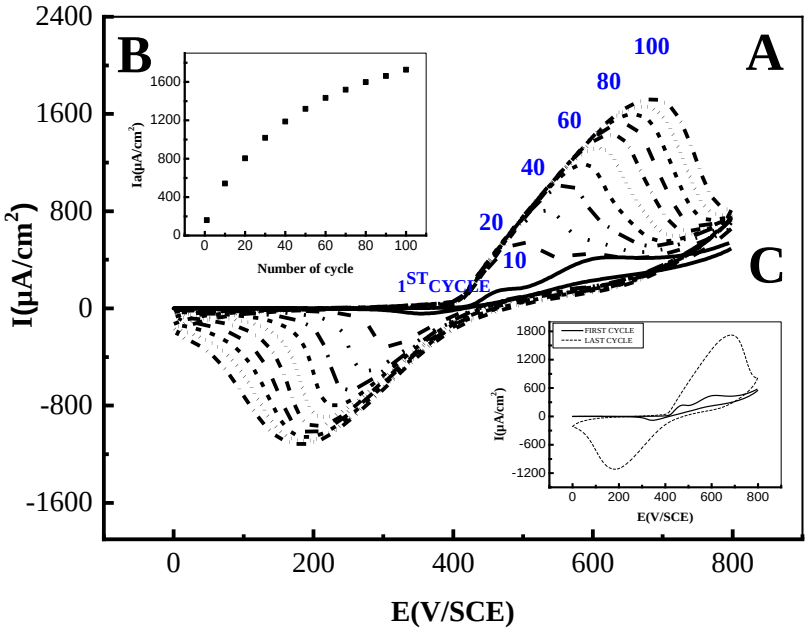

Figure 6. (A) Cyclic voltammograms of [Ni(II)-L-pyridine]Cl/ITO modified electrode in (10^{-1} M NaCl, 10^{-1} M NaOH, pH = 11) alkaline solution at 100 V/s. Scans 10, 20, 30, 40, 50, 60, 70, 80, 90, and 100 are shown: (B) The insert shows the anodic peak current vs number of cycles for the oxidation peak, (C) first scan and last scan.

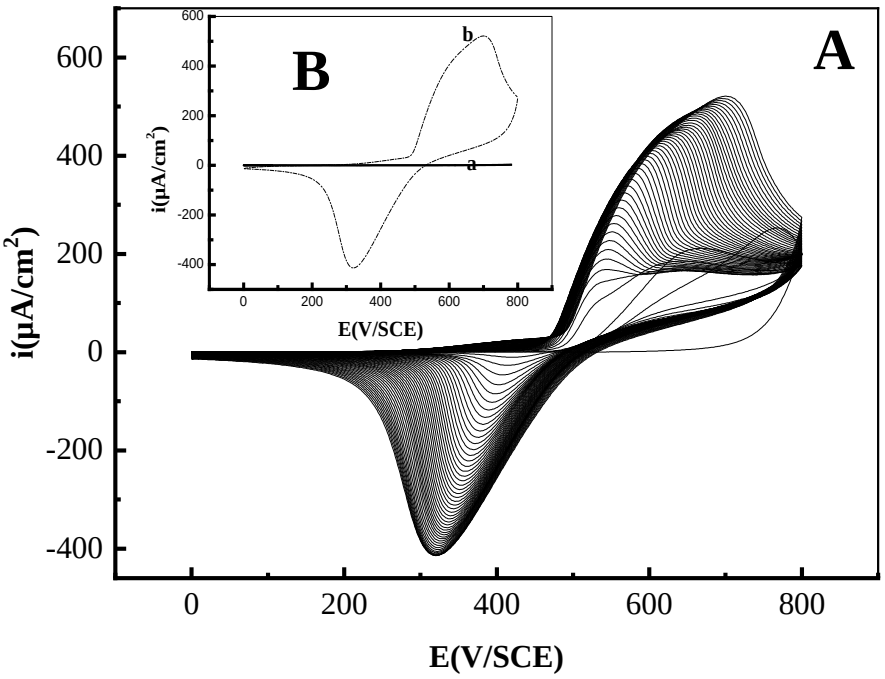

Figure 7. (A) Synthesis of electroactive film of nickel compounds (50 cycles) on FTO in alkaline solution (10^{-1}M NaCl, 10^{-1} M NaOH, pH = 11) containing 10^{-3} M of [Ni(II)-L-pyridine]Cl; v = 100 mVs^{-1}. Inset (B): unmodified FTO electrode (a), cyclic voltammogram of the film of nickel compounds (50 cycles) in the alkaline solution; v = 100 V s^{-1}, modified FTO electrode (b).

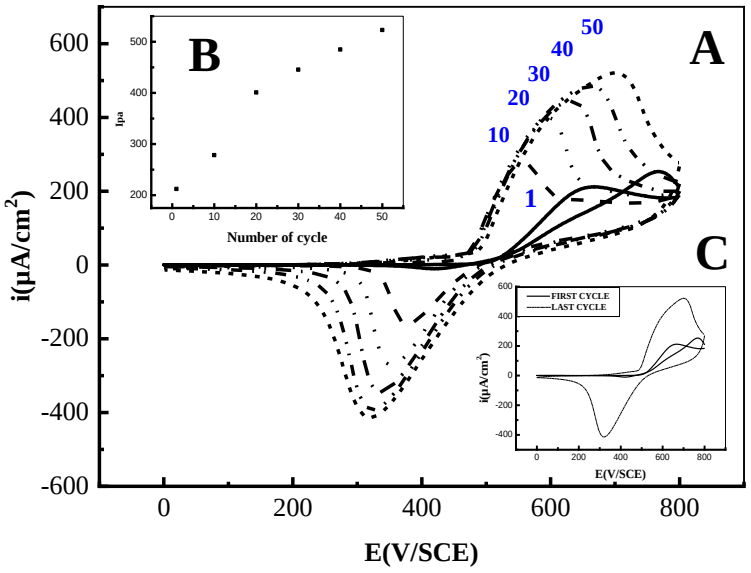

Figure 8. (A) Cyclic voltammograms of [Ni(II)-L-pyridine]Cl/ITO modified electrode in (10^{-1} M NaCl, 10^{-1} M NaOH, pH = 11) alkaline solution at 100 V/s. Scans 10, 20, 30, 40 and 50 are shown. (B) The insert shows the anodic pic current vs number of cycles for the oxidation peak, (C) first scan and last scan.

3.3. SEM characterization

The surface morphology was patterned by the scanning electron microscopy (SEM). The SEM analyses of the synthesized nickel complex were explored via micrographs obtained, by using films of [Ni(II)-L-pyridine]Cl electrodeposited on ITO substrate, represented in Fig. 9 (A-D). Regarding those obtained on the FTO substrate are illustrated in Fig. 9 (E-H). It can be seen from the SEM images of Ni(II) complex, electrodeposited on the both substrates the presence of some non-uniform platelet morphology with variable lateral dimensions. The observed particles sizes of the Ni(II) complex were found to have diameters more than 100 nm after 100 cycles. This result seems to coincide with an unexpected increase in the current density of the cyclic voltammograms due to the non-uniform growing of grain size obtained. However, the next following cycles cause a significant increase in the grain size inducing a neat enhancement of the roughness of the resulting film as represented in the electrode surface, obtained after 100 cycles on ITO substrate [46,47].

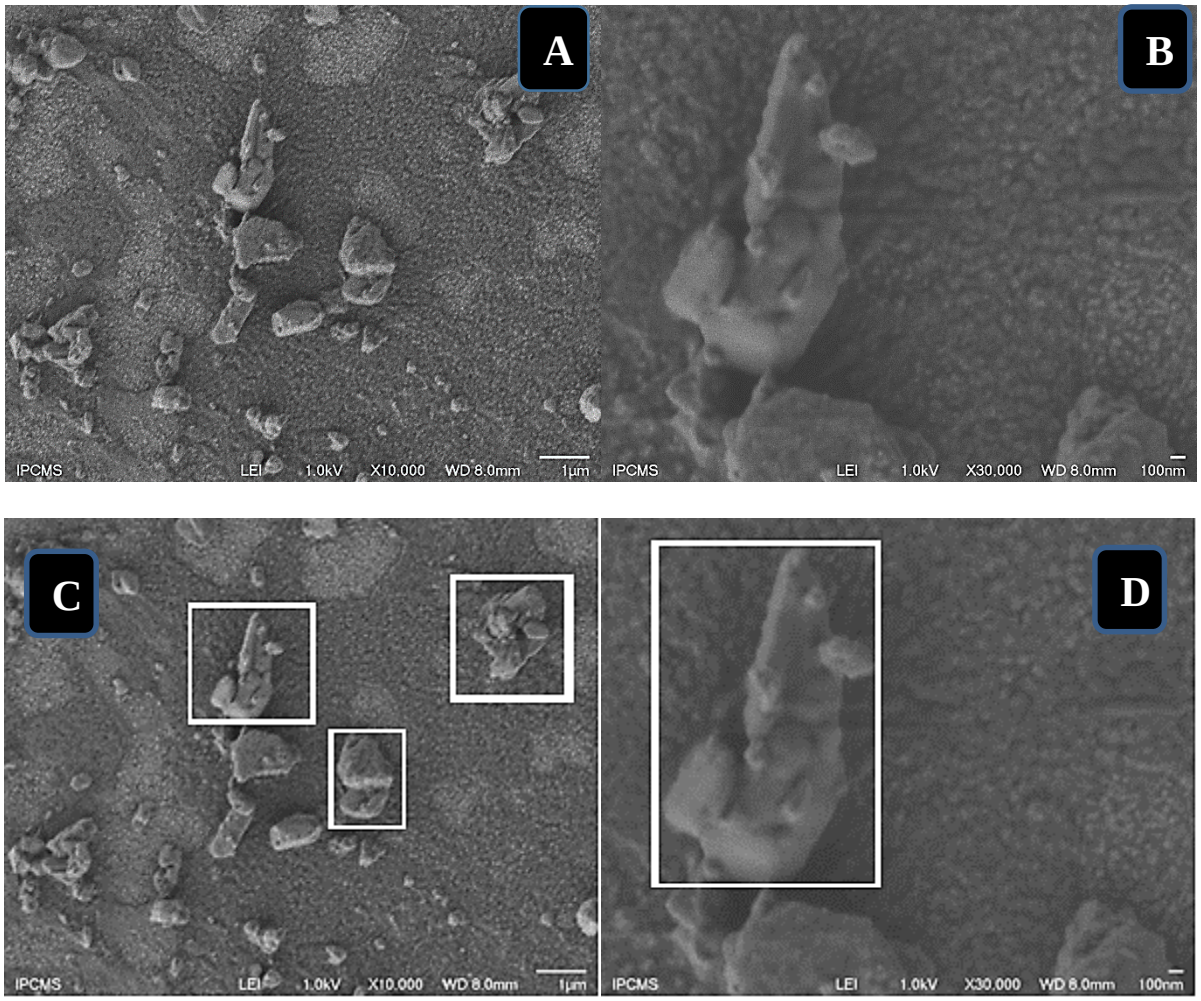

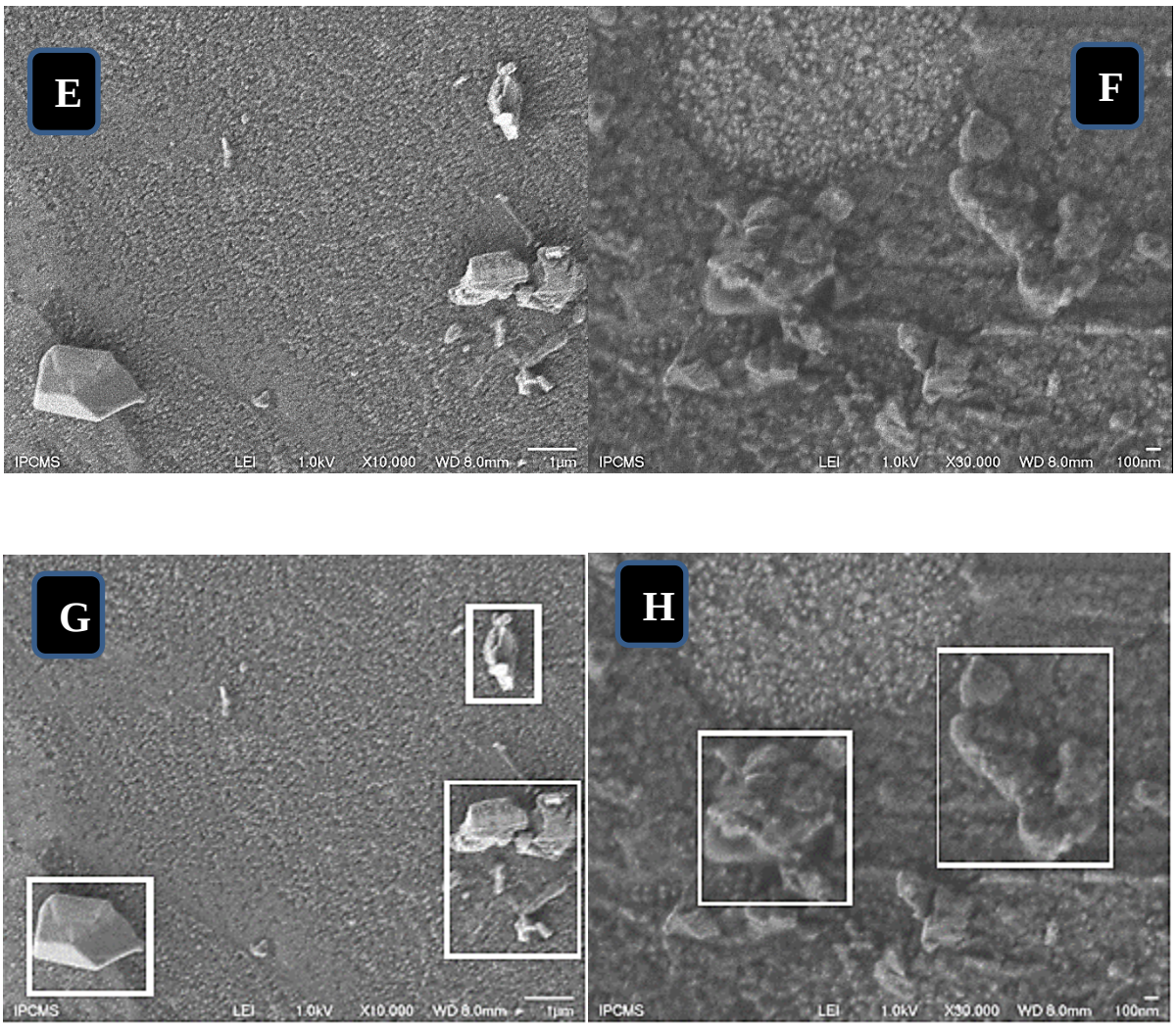

Figure 9. Scanning electron micrographs of [Ni(II)-L-pyridine]Cl complex electrodeposited on ITO substrate (A-D) and on FTO substrate (E-H).

3.4. XPS characterization

X-ray photoelectron spectroscopy (XPS) was used to study the molecular structures in their solid phase or polymeric forms. So, surface compositions of [Ni(II)-L-pyridine]Cl (Fig. 10A) and poly-[Ni(II)-L-pyridine]Cl/ITO (Fig. 10B) was examined to determine the character of the electron density distribution. XPS spectra reveal the content of these materials as elemental analysis like chlorine, carbon, nitrogen, oxygen and Ni either in the nickel complex powder or in its films electrodeposited onto ITO substrate (Fig. 10). Based on these analyses, some kinetic energy shifts were observed for polymer but, the nickel as metal was found to be approximately present at the same level in the both cases. The Ni coverage appeared obviously as higher in powder form than in its polymeric films. The spectrum of poly-[Ni(II)-L-pyridine]Cl/ITO was also supported by the presence of indium tin oxide composition (Si 2p, In 3p, Sn 3p). Fig. 10B, the Ni-2p can be seen on the spectrum as very weak signal when its films were analyzed.

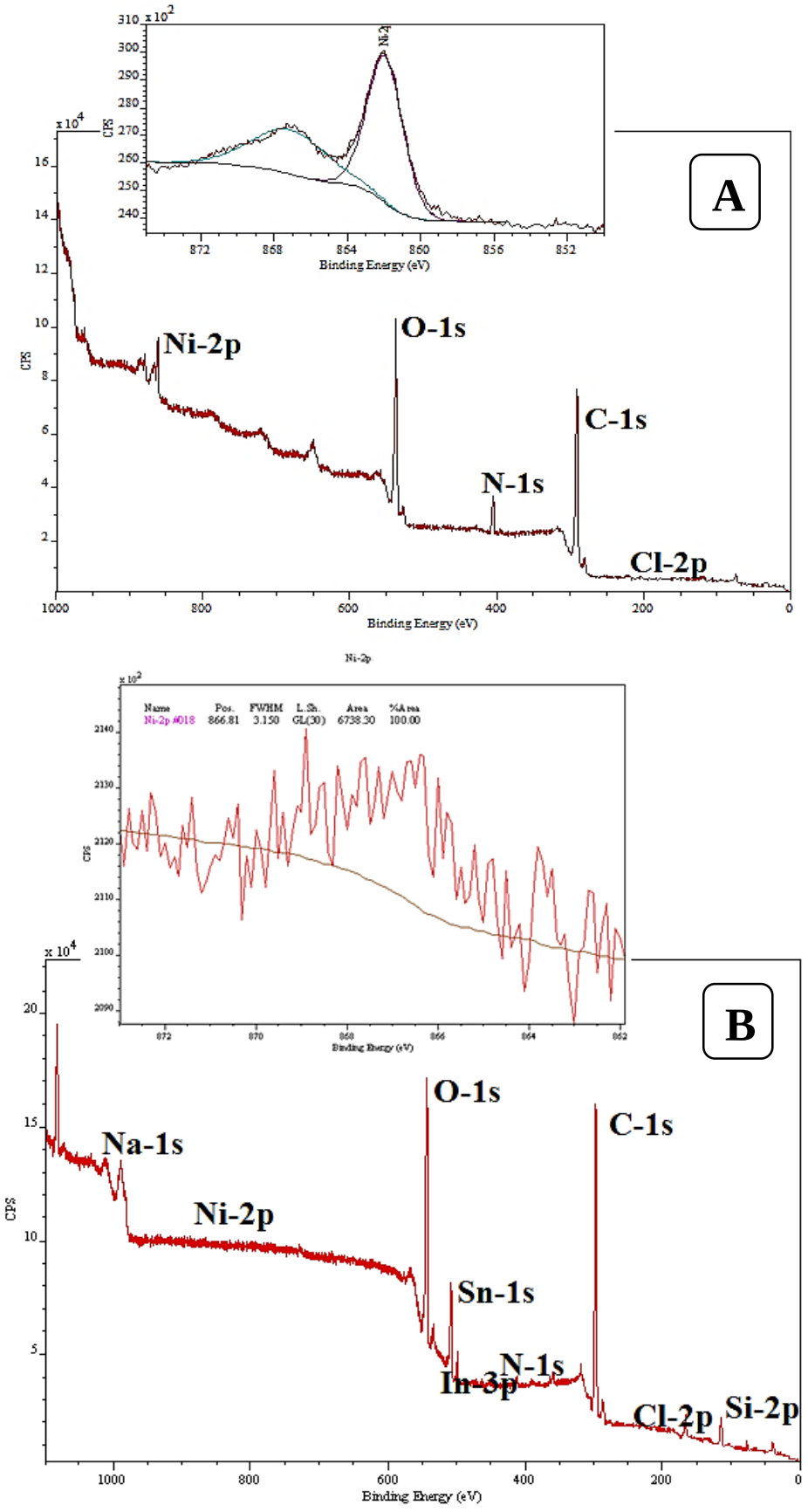

Figure 10. XPS spectra of: (A) Ni(II)-L-pyridine]Cl complex powder, (B) poly-Ni(II)-L-pyridine]Cl/ITO films.

This could be attributed to the formation of $Ni(OH)_2$ hydroxides in the bulk of polymer film. By using electrochemical behavior, Nickel oxide (NiO) is acknowledged to be formed in very small quantities and to be associated to surface passivation. The XPS results suggest that the electrodeposited Ni metal is progressively transformed to the Ni hydroxides [48,49].

3.5. Electrocatalytic oxidation of aliphatic alcohols

3.5.1. Electro-oxidation of methanol with poly-[Ni(II)-L-pyridine]Cl/GC Electrode

The electrocatalytic activity of Poly-[Ni(II)-L-pyridine]Cl film was attempted to investigate the oxidation reaction of MeOH using cyclic voltammetry. Typical cyclic voltammograms of poly-[Ni(II)-L-pyridine]Cl/GC electrode, immersed in 0.1 M NaOH solution without MeOH (a), with 0.625 M MeOH (b) and with 5 M of MeOH (c) with applying 100 mVs^{-1} as scan rate. The voltammetric curves resulting are presented in Fig. 11. Regarding the case where this GC modified electrode immersed in the electrolytic solution no containing MeOH, only the redox couple (Ni^{II}, Ni^{III}) was observed on the cyclic voltammogram without anyone electrocatalytic effect (See curve a) of ([Ni(II)-L-pyridine]Cl)/([Ni(III)-L-pyridine]Cl) as reported in the literature [50,51]. Accordingly, it can be obviously distinguished that the anodic wave practically disappears at the highest concentrations. This shows clearly that Ox-species of nickel were involved in chemical reaction rendering it non-reversible.

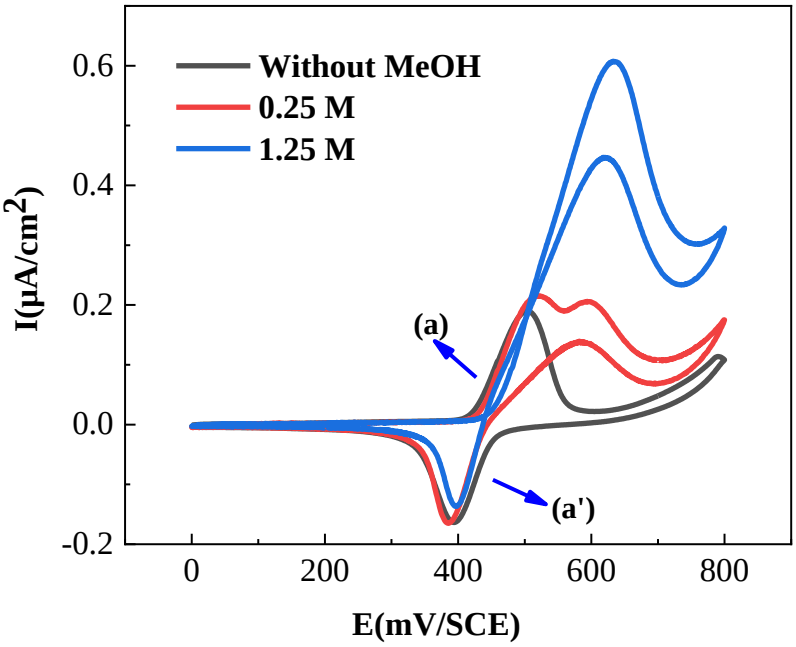

Figure 11. Voltammetric curves of methanol oxidation on a poly-[Ni(II)-L-pyridine]Cl/GC electrode at scan rate of 100 mVs^{-1} in 0.1 M NaOH solution containing: 0, 0.25 and 1.25 M of MeOH.

In addition, the catalytic peak current observed at +0.700 V shows a reasonable modification that can be related to a gradual increase in the peak current. Thus, at high concentrations, it seems that all catalytic sites of Ni(III)-L in the film of the modified electrode are systematically reduced by molecules

of the used alcohol as a substrate as it has been well discussed in the literature [52]. This result is in good agreement with interactions of MeOH molecules towards electro-catalytic sites indicating the limiting step of the mechanism governing this oxidation reaction [53]. This explains the total disappearance of the both peak currents (a) and (a') [54].

Fig. 12 shows the cyclovoltammogram of poly-[Ni(II)-L-pyridine]Cl/GC film of ME with different concentrations of MeOH. So, this ME was placed in a clean electrochemical cell containing a 0.1 M NaOH solution with diverse concentrations of MeOH varying from 0.0 to 10 M. The peak current of each one of this oxidation reaction increase progressively according the concentration of MeOH up to the value 1.25 M which can be explained by a progressive diminution due to the saturation of catalytic sites on the surface of the modified electrode.

Based on this assessment, it can be concluded that the formation of poly-[Ni(II)-L-pyridine]Cl/GC plays a vital catalytic role towards the oxidation reaction of MeOH according the following possible mechanisms:

Poly-[$Ni(OH)_2$-L-pyridine] + OH- → Poly-[Ni(OOH)-L-pyridine] + H_2O + e-.

Poly-[Ni(OOH)-L-pyridine] + MeOH → Product + poly-[$Ni(OH)_2$-L-pyridine].

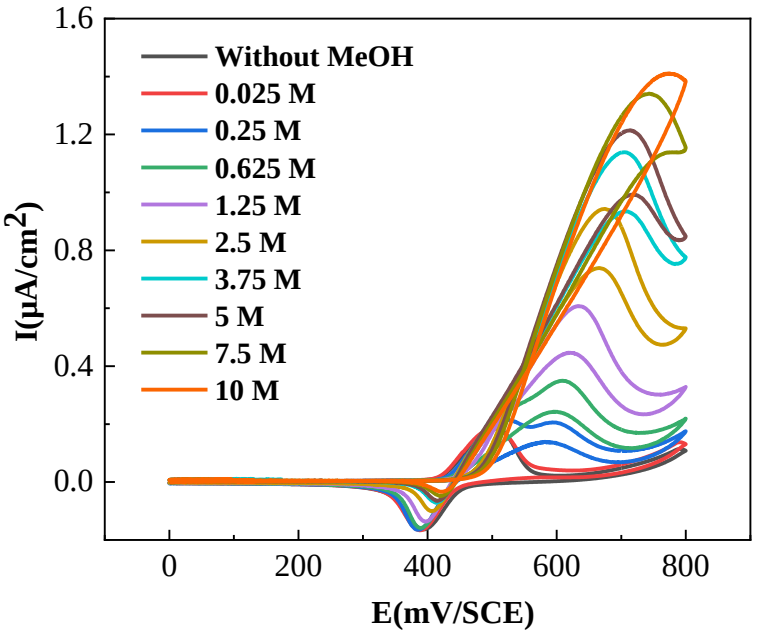

Figure 12. Voltammetric curves of MeOH oxidation on a poly-[Ni(II)-L-pyridine]Cl/GC electrode at scan rate of 100 mVs^{-1} in 0.1 M NaOH solutions containing methanol as follows: 0, 0.025, 0.25, 0.625, 1.25, 2.5, 3.75, 5, 7,5 and 10 M.

3.5.2. Electro-oxidation of ethanol at poly-[Ni(II)-L-pyridine]Cl /GC electrode

Fig. 13 shows the cyclic voltammogram of poly-[Ni(II)-L-pyridine]Cl/GC modified electrode, it was placed in a fresh electrochemical cell containing a 0.1 M NaOH solution. The concentration of EtOH has been varied in the range from 0.0 to 5.16 M. In this figure, the catalytic effect of the electrochemical

oxidation reaction of EtOH molecules appears even at low concentrations. Therefore, the increase in anodic peak of Ni(II)/Ni(III) redox system and the appearance of the second wave of oxidation of EtOH from the first addition has been observed. At low concentrations, two waves of potentials (Epa_I, Epa_{II}) are observed, expressing the oxidation of EtOH between two potentials zones. At high concentrations of EtOH, we have noted that the first wave tends to disappear in favor of the second. This is also accompanied by a displacement of the oxidation potentials of EtOH molecules. Such shift in potentials can be explained by a higher resistance to electron transfer between nickel sites in the polymeric matrix due to the adsorption of EtOH molecules on nickel metal centers [55]. In this case, we note that as the concentration of EtOH increases, the peak currents increase linearly with the concentration of the substrate up to the value 3.14 M which corresponds to the appearance of a decrease in peak current Ipa that can be assigned to the saturation of the catalytic sites of the modified electrode [56,57]. During the catalytic process of EtOH oxidation on the modified electrode, we have observed a gradual disappearance of the Ipa^{II} oxidation wave to the benefit of this oxidation, which shows that the nickel Ox species, present in the poly-[Ni(II)-L-pyridine]Cl/GC film, undergo a chemical reaction making the electrochemical process non-reversible as indicated in the following reaction mechanism.

Poly-[$Ni(OH)_2$-L-pyridine] + OH- → Poly-[Ni(OOH)-L-pyridine] + H_2O + e-.

Poly-[Ni(OOH)-L-pyridine] + EtOH → Product + poly-[$Ni(OH)_2$-L-pyridine].

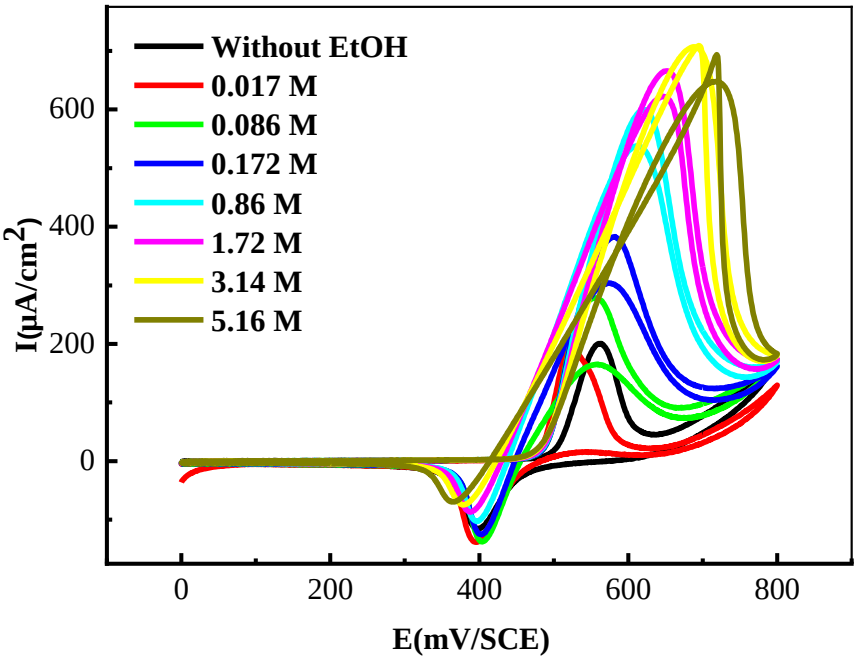

Figure 12. Voltammetric curves of EtOH oxidation on a poly-[Ni(II)-L-pyridine]Cl/GC electrode at scan rate of 100 mVs^{-1} in 0.1 M NaOH solution containing EtOH as follows: 0, 0.0172, 0.086, 0.172, 0.86, 1.72, 3.14, 5.16 M.

3.5.3. Electro-oxidation of isopropanol at poly-[Ni(II)-L-pyridine]Cl/GC electrode

Cyclic voltammograms of [Ni(II)-L-pyridine]Cl recorded in 0.1M NaOH solutions at 100 mVs^{-1} as scan rate for various ^{i}PrOH concentrations between 0 to 26 mM are shown in Fig. 13. As can be seen in this figure, the ^{i}PrOH oxidation onset potentials increase with increasing ^{i}PrOH concentration. Consequently, high numbers of Ni(II) active centers have been resulted by increasing the alcohol concentrations. In the 0 – 0.5 M concentration range of this alcohol, a linear relationship between the anodic peak current and ^{i}PrOH concentration is observed and also the peak potentials shift positively with increasing of the alcohol concentration. These obtained results suggest that the electro-catalytic oxidation is controlled by the diffusion of the reactant in the heart of the modified electrode.

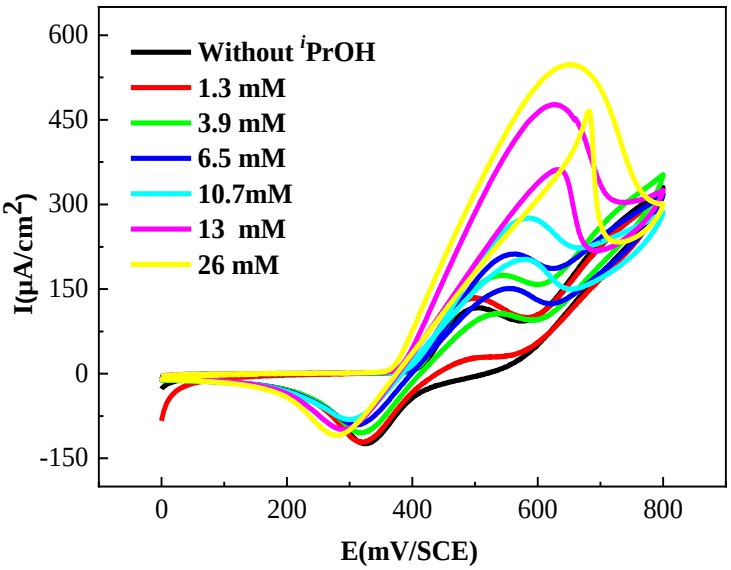

Figure 13. Cyclic voltammograms of ^{i}PrOH oxidation on a poly-[Ni(II)-L-pyridine]Cl/GC electrode at scan rate of 100 mVs^{-1} in 0.1 M NaOH solution containing ^{i}PrOH as follows: 0, 1.3, 3.9, 6.5, 10.7, 13 and 26 mM.

4. CONCLUSIONS

The initial results obtained from this study are: (1) The synthesized and characterized Ni(II)-Unsymmetrical Schiff Base complex noted [Ni(II)-L-pyridine]Cl is successively electropolymerized onto glassy carbon, indium tin oxide and fluorine tin oxide electrodes. (2) The obtained films present a high adherence and good stability. (3) The attained modified electrodes present only one redox system attributed to the ([Ni(II)-L-pyridine]Cl)/([Ni(III)-L-pyridine]Cl) redox couple. (4) By using alkaline medium, the [Ni(II)-L-pyridine]Cl GC modified electrodes have a strong electrocatalytic oxidation activity towards some aliphatic alcohols such as methanol, ethanol and isopropanol. (5) A diffusional catalytic process was obtained at low alcohol concentrations. In the case of high alcohol concentrations, the reaction is directed by a kinetic interaction between the oxidized nickel catalytic centers, distributed

in the heart of the polymer film and alcohol molecules. As last conclusion, these modified electrodes can be adventured in the electro-oxidation of other kind of alcohols, such as the aromatic ones.

ACKNOWLEDGEMENTS
The authors thank the Algerian Ministry of Higher Education and Scientific Research (MESRS) and the Director General for Scientific Research and Technological Development (DGRSDT) for the financial support.

References

1. J.P. Zhao, D.W.Y. Hernández, D.W. Zhou, D.Y. Yang, D.E.I. Vovk, D.M. Capron, D.V. Ordomsky, *ChemCatChem*, 12 (2020) 238.
2. W.-Y. Tan, Y. Lu, J.-F. Zhao, W. Chen, H. Zhang, *Org. Lett.*, 23 (2021) 6648.
3. (A) D. Pletcher, *J. Appl. Electrochem.*, 14 (1984) 403; (B) K.L. Walker, L.M. Dornan, R.N. Zare, R.M. Waymouth, M.J. Muldoon, *J. Am. Chem. Soc.*, 139 (2017) 12495.
4. A. Ciszewski, G. Milczarek, *J. Electroanal. Chem.*, 426 (1997) 125.
5. A. Ciszewski, G. Milczarek, *J. Electroanal. Chem.*, 413 (1996) 137.
6. M.S. Ureta-Zanartu, C. Berrios, J. Pavez, J. Zagal, C. Gutierrez, J.F. Marco, *J. Electroanal. Chem.*, 553 (2003) 147.
7. M. Manriquez, J.L. Bravo, S. Gutierrez-Grandos, S.S. Succar, C. Bied-Charreton, A.A. Ordaz, F. Bedioui, *Anal. Chim. Acta*, 378 (1999) 159.
8. F. Bedioui, *Coord. Chem. Rev.*, 144 (1995) 39.
9. J. Obirai, F. Bedioui, T. Nyokong, *J. Electroanal. Chem.*, 576 (2005) 323.
10. B.M. Johnson, R. Francke, R.D. Little, L.A. Berben, *Chem. Sci.*, 8 (2017) 6493.
11. R. Rajeev, B. Sharma, A.T. Mathew, L. George, S. Yn, A. Varghese, *J. Electrochem. Soc.*, 167 (2020) 136508.
12. G.V. Lima, L.S. Mello, E.R. Dockal, M.F. Oliveira, *Food Chem.*, (2022) 132271.
13. A.N. Golikand, S. Shahrokhian, M. Asgari, A. Khanchi, *J. Power Sources*, 144 (2005) 21.
14. M. Noroozi, S.G. Saremi, *Iran. J. Chem. Chem. Eng.*, 40 (2020) 1395.
15. D. Tomczyk, W. Bukowski, K. Bester, M. Kaczmarek, *Materials*, 15 (2022) 191.
16. J.L. Bott-Neto, T.S. Martins, S.A.S. Machado, E.A. Ticianelli, *ACS Appl. Mater. Interfaces*, 11 (2019) 30810.
17. S. Trevin, F. Bedioui, M.G.G. Villegas, C. Bied-Charreton, *J. Mater. Chem.*, 7 (1997) 923.
18. P.E. Martínez, B.N. Martínez, C.R. de Barbarín, *Adv. Tech. Mat. Mat. Proc.*, 8 (2006) 41.
19. J. Losada, I. del Peso, L. Beyer, *J. Electroanal. Chem.*, 447 (1998) 147.
20. R. Benramdane, F. Benghanem, A. Ourari, S. Keraghel, G. Bouet, *J. Coord. Chem.*, 68 (2015) 560.
21. N. Bounab, A. Ourari, W. Derafa, Djouhra Aggoun, *J. Fundam. Appl. Sci.*, 11 (2019) 492.
22. Z. He, J. Chen, D. Liu, H. Zhou, Y. Kuang, *Diam. Relat. Mater.*, 13 (2004) 1764.
23. H. Nonaka, Y. Matsumura, *J. Electroanal. Chem.*, 520 (2002) 101.
24. G. Roslonek, J. Taraszewska, *J. Electroanal. Chem.*, 325 (1992) 285.
25. M. Brodt, K. Müller, J. Kerres, I. Katsounaros, K. Mayrhofer, P. Preuster, P. Wasserscheid, S. Thiele, *Energy Technol.*, 9 (2021) 2100164.
26. M. Jafarian, M. Babaee, F. Gobal, M.G. Mahjani, *J. Electroanal. Chem.*, 652 (2011) 8.
27. E. Rotondo, F.C. Priolo, *J. Chem. Soc. Dalton Trans.*, 9 (1982) 1825.
28. A. Ourari, W. Derafa, D. Aggoun, *RSC Adv.*, 5 (2015) 82894.
29. M. Morshedi, M. Aminasr, A.M.Z. Slawin, J.D. Woollins, A.D. Khalaji, *Polyhedron*, 28 (2009) 167.
30. M. Aslantas, E. Kendi, N. Demir, A.E. Sabik, M. Tumer, M. Kertmen, *Spectrochim. Acta Part A*,

74 (2009) 617.
31. D. Aggoun, Z. Messasma, B. Bouzerafa, R. Berenguer, E. Morallon, Y. Ouennoughi, A. Ourari, *J. Mol. Struct.*, 1231 (2021) 129923.
32. M. Abdel Azzem, Z.F. Mohamed, H.M. Fahmy, *J. Electroanal. Chem.*, 399 (1995) 121.
33. U.S. Yousef, *Eur. Polym. J.*, 35 (2000) 133.
34. U.S. Yousef, *Eur. Polym. J.*, 36 (2000) 1629.
35. W. Belbacha, F. Naamoune, H. Bezzi, N. Hellal, L. Zerroual, K. Abdelkarim, B. Bouzarafa, M. Fernandez Garcia, D. Lopez, *Arab. J. Chem.*, 13 (2020) 6072.
36. A. Ourari, N. Hellal, N. Charef, D. Aggoun, *Electrochim. Acta*, 170 (2015) 311.
37. M. Revenga-Parra, T. Garcıa, E. Lorenzo, F. Pariente, *Sensors Actuat. B*, 130 (2008) 730.
38. C.P. Andrieux, J.M. Saveant, *J. Electroanal. Chem.*, 111 (1980) 377.
39. E. Laviron, *J. Electroanal. Chem.*, 101 (1979) 19.
40. (A) S. Antoniadou, A.D. Jannakoudakis. E. Theodoridou, *Synth. Met.*, 30 (1989) 295; (B) S. Karp, L. Meites, *J. Am. Chem. Soc.*, 84 (1962) 906.
41. S.M. Golabi, A. Nozad, *Electroanalysis*, 16 (2004) 199.
42. T. Malinski, A. Ciszewski, J. Bennett, J.R. Fish, L. Czuchajowski, *J. Electrochem. Soc.*, 138 (1991) 2008.
43. M. Revenga-Parra, T. Garcıa, E. Lorenzo, F. Pariente, *Sensor Actuat. B-Chem.*, 130 (2008) 730.
44. I.C. Santos, M. Vilas-Boas, M.F.M. Piedade, C. Freire, M.T. Duarte, B. de Castro, *Polyhedron*, 19 (2000) 655.
45. A. Ourari, D. Aggoun, *J. Iran. Chem. Soc.*, 12 (2015) 1893.
46. J.S. Jeon, I.K. Yu, W. Kim, S.H. Choi, *Front. Chem.*, 8 (2020) 595616.
47. A. Ourari, B. Ketfi, and L. Zerroual, *Arab. J. Chem.*, 10 (2017) 914.
48. S.H. Kazemi, R. Mohamadi, *Electrochim. Acta*, 109 (2013) 823.
49. M.S. Ureta-Zanartu, C. Berrıos, J. Pavez, J. Zagal, C. Gutierrez, J.F. Marco, *J. Electroanal. Chem.*, 553 (2003) 147.
50. A. Ourari, D. Aggoun, L. Ouahab, *Inorg. Chem. Commun.*, 33 (2013) 118.
51. J.B. Raoof, M.A. Karimi, S.R. Hosseini, S. Mangelizadeh, *Electroanal. Chem.*, 638 (2010) 33.
52. M. Jafarian, R.B. Moghhaddam, M.G. Mahjani, F. Gobal, *J. Appl. Electrochem.*, 36 (2006) 913.
53. R. Ojani, J.B. Raoof, S. Fathi, *Electrochim. Acta*, 54 (2009) 2190.
54. I. Danaee, M. Jafarian, F. Forouzandeh, F. Gobal, M.G. Mahjani, *Int. J. Hydrogen Energ.*, 33 (2008) 4367.
55. A. Bezza, Y. Ouennoughi, B. Bouzerafa, D. Aggoun, H. Bezzi, D. Lopez, M. Fernandez-Garcıa, A. Ourari, *Res. Chem. Intermed.*, 44 (2018) 6831.
56. H.G. Meier, J.R. Vilche, A.J. Arvia, *J. Appl. Electrochem.*, 10 (1980) 611.
57. M. Jafarian, M.A. Haghighatbin, F. Gobal, M.G. Mahjani, S. Rayati, *J. Electroanal. Chem.*, 663 (2011) 14.